Zn-Modified In2O3 Nanoparticles: Facile Synthesis, Characterization, and Selective Cytotoxicity against Human Cancer Cells

by Virtual Research Cooperative

Submission date: 10-Nov-2023 12:43PM (UTC-0500)
Submission ID: 2223291442
File name: Revised_Ms_-II.docx (3.21M)
Word count: 5705
Character count: 33362

Zn-Modified In_2O_3 Nanoparticles: Facile Synthesis, Characterization, and Selective Cytotoxicity against Human Cancer Cells

Abstract

Oxide nanoparticles (NPs) have attracted considerable interest owing to their unique characteristics and possible applications, including gas detection, bioanalytical sensing, catalytic, and biomedical. The present work was designed to explore the effect of varying amounts of Zn-doping on the properties and selective anticancer efficacy of In_2O_3 NPs. The precipitation process was applied to prepare pure In_2O_3 NPs and Zn-doped In_2O_3 NPs. XRD, TEM, SEM, EDX, XPS, UV-Vis, and PL techniques have been employed to investigate the physicochemical properties of NPs. The XRD analysis revealed that the crystallite of the In_2O_3 lattice was slightly changed with the addition of Zn ions. TEM and SEM images displayed that the reduction of size of In_2O_3 NPs was increased with increasing Zn concentrations. The composition elements and distribution of Zn dopants within In_2O_3 NPs were further confirmed by EDX and XPS techniques. Based on the UV-Vis study, increasing the Zn amount improved the gap energy of In_2O_3 NPs by shifting edge absorption peaks to lower wavelengths. Moreover, PL spectra show that the intensity of In_2O_3 NPs decreased with increasing the Zn amount. The biological results indicate that the Zn-doped In_2O_3 NPs exhibited a significant increase in cytotoxicity with Zn doping increased against MCF-7 HCT116) cells while they have excellent biocompatibility with normal human cells (HUVECs). These results suggest that these NPs hold promise as a novel therapeutic approach in cancer treatment. This study requires more research into the biological applications of Zn-doped In_2O_3 NPs.

Keywords: Precipitation process, Zn doping, Anticancer Activity, Physicochemical Properties, and Selective Cytotoxicity.

1.Introduction

Nanotechnology has attracted interest in the biomedical field as a novel approach for addressing some challenges in healthcare problems, such as drug delivery and cancer therapy (Jahan, 2022; Patel and Nanda, 2015; Sun et al., 2014; Yang et al., 2022). Currently, enhanced nanomaterials provide tailored cancer therapies that maximize therapeutic efficiency owing to their superior properties (Gao et al., 2019; Navya et al., 2019). Oxide nanoparticles (NPs) are now being studied of significant interest within nanomaterials due to their exceptional mechanical, electronic, and catalytic characteristics. These properties make them very promising in potential applications such as sensing, electronics, and biomedicine (Malini et al., 2022; Mishra et al., 2017; Sheena et al., 2019). For example, Indium oxide (In_2O_3) is a crucial n-type semiconductor with a band gap ranging from 3 to 3.75 eV (Bierwagen, 2015). Owing to its biocompatibility, low toxicity, and tunable bandgap, it has emerged as an attractive candidate in potential applications, including industrial, catalytic , electronics, and biomedical applications (Z. A. M. Alaizeri et al., 2022; Li et al., 2020; Yang et al., 2022).

The doping of oxide NPs has opened new research paths in numerous fields. For example, doping oxide NPs with transition metal ions can significantly affect their physicochemical properties and performance (Ahamed et al., 2016). For instance, In_2O_3 NPs NPs have been doped with metal ions (e.g., Zn, Co, and Ag) to improve their properties ("Ac ce d M us," 2019; Sun et al., 2016; Yan et al., 2018). Different physical, chemical, and biological approaches were successfully applied to achieve doping In_2O_3NPs with transition metal ions (Kulkarni and Patil, 2016; Naik and Salker, 2017). Shanmuganathan et al. (Shanmuganathan et al., 2021) reported that a 1wt% of Mn, Fe, Co, Ni, and Cu were doped to In_2O_3 nanostructures using a hydrothermal process to enhance photocatalytic activity. In another study, Sn-doped In_2O_3 NPs synthesized using a sol–gel combustion method (Ayeshamariam et al., 2014).

Several studies are attracting attention in using metal-doped oxide NPs in biomedicine applications because to their superior properties. However, modifying these NPs with zinc (Zn) can enhance their properties, potentially improving their efficacy in cancer therapy. Sharma et al. (Sharma et al., 2022) investigated that Zn doping improves the

physicochemical characteristics of WO_3 NPs for biosensing, imaging, antibacterial, and anticancer medicine. Darvish et al. (Darvish et al., 2022) observed that human lung (A549) cancer cells responded better to doping Zn on $CuFe_2O_4$ NPs than to $CuFe_2O_4$ NPs. The improved therapeutic efficacy and reduced systemic toxicity by using Fe-doped ZnO NPs in a murine tumor model demonstrated by Zhao et al. (Zhao et al., 2018). Our previous work (Z. A. M. Alaizeri et al., 2022) investigated that the Ag adding has a role in the improved photocatalytic and anticancer performance of In_2O_3 NPs. Additionally, Karmaoui et al. (Karmaoui et al., 2016)found that Pt-decorated In_2O_3 NPs display high sensitivity in detecting acetone and a biomarker for diabetes. Vázquez-Olmos et al.(Vázquez-Olmos et al., 2014)synthesized Mn-doped In_2O_3 NPs and found evidence of paramagnetic centers, suggesting potential applications in diluted magnetic semiconductor

The goal of the present work was to evaluate the influence of Zn doping on the physicochemical and anticancer properties of In_2O_3 NPs. Pure In_2O_3 NPs and Zn-doped In_2O_3 NPs were prepared through chemical precipitation. The physicochemical properties of the prepared NPs were investigated through XRD, TEM, SEM, EDS, XPS, UV-vis, and PL Spectrometer. Anticancer activity of synthesized NPs was evaluated using different types of human cancer cells (MCF-7 and HCT116). Furthermore, the biocompatibility of the prepared nanoparticles was assessed by HUVE normal cells. In vitro study results showed that In vitro study showed that Zn doping increases selective anticancer efficacy of In_2O_3 NPs against human normal (HUVEs) and different types of cancer cells(MCF-7 and HCT116).

2. Experimental details

2.1 Chemicals, reagents, and cells

Indium chloride ($InCl_3$) (purity of 98%), zinc chloride ($ZnCl_2$) (minimum purity of 98%, and ammonium hydroxide (NH_4OH) (a concentration of 28.0-30.0% NH_3 basis) were supplied from Sigma Aldrich (Millipore-Sigma, St. Louis, MO, USA). MTT (6-[4,5-dimethylthiazol-2-yl]-2,5-diphenyl-tetrazolium bromide), and foetal bovine serum (FBS) were provided from Sigma Aldrich (Millipore-Sigma, St. Louis, MO, USA). The human breast (MCF-7)and colorectal (HCT116) cancer cells were acquired from the American (

ATCC, Manassas, West Virginia, USA). The human umbilical vein endothelial cells (HUVECs) were received from the microbiology Lab at King Saud University (KSU).

2.2 Synthesis of Zn-doped In_2O_3 NPs

Zn-doped In_2O_3 NPs were successfully synthesized using a chemical precipitation process as in an earlier study (Zheng et al., 2021). The 3.6mmol of indium chloride ($InCl_3$) was prepared in 20 ml of ethanol and 10 ml of distilled water under stirring for 20 min at 70 °C on a hot plate. Next, different amount (2.5%, 5%, and 7.5 mol%) zinc chloride ($ZnCl_2$) was dropwise added to the solution with stirring. After that, a 2 M solution of ammonium hydroxide (NH_4OH) was also gradually added to reach a pH of around 9 under continuous stirring for 4 h to get precipitate. Subsequently, The precipitate was rinsed repeatedly with distilled water and ethanol and centrifuged at 7000 rpm for 5 min to separate it from the solution. The rinsed precipitate was then dried at 70 °C for 12 h and annealed at 450 °C for 2 h. At a similar protocol, pure In_2O_3 NPs were successfully synthesized. The above procedure of synthesis of Zn-doped In_2O_3 NPs was illustrated in Scheme 1.

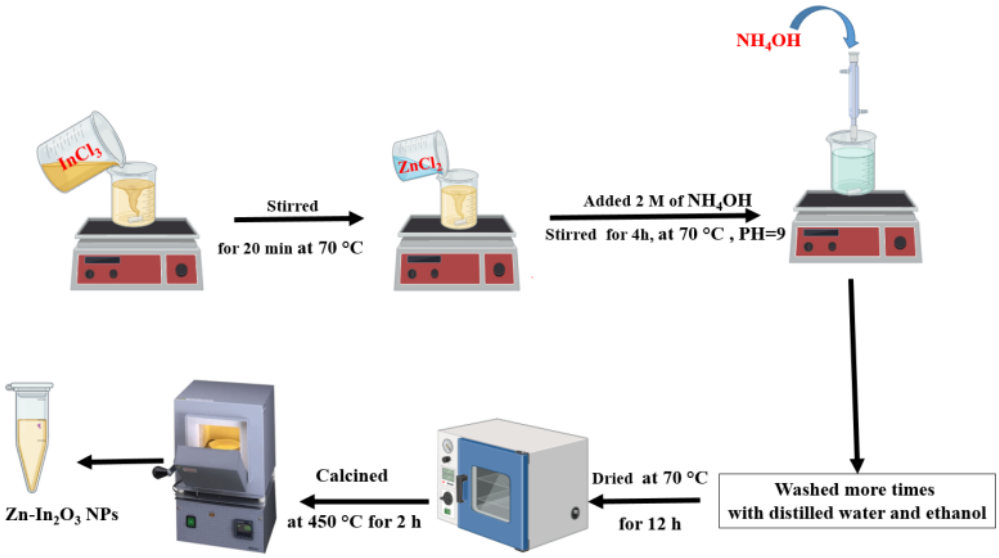

Scheme 1: The procedure of synthesis of Zn-doped In_2O_3 NPs.

2.3 Characterization

X-ray diffraction (XRD) patterns (PanAnalytic X'Pert Pro from Malvern, UK, with Cu-Kα radiation (wavelength = 0.15405 nm) at 45 kV and 40 mA) were used to examine phases and crystal structure of prepared NPs. Moreover, field emission transmission electron microscopy (FE-TEM) (JEM-2100F, JEOL, Inc., Tokyo, Japan) was used to determine particle size of NPs. Moreover, field emission scanning electron microscopy (FE-SEM) (JSM-7600F, JEOL,93Inc) was applied to investigate shape and surface morphology of these NPs. We used EDX and XPS (PHI-5300 ESCA PerkinElmer, Boston, MA) to confirm elemental amnalysis and chemical states of samples. UV-Visible spectrometer (Hitachi U-2600) and PL spectrometer (Hitachi F-4600) were employed to measure optical characteristics.

2.4 Cells culture

MCF-7 and HCT116 cancer cells were cultured in Dulbecco Modified Broker Eagle Medium (DMEM) with 10% fetal bovine serum (FBS) and antibiotics (100 µg/mL streptomycin and 100 U/mL penicillin). Cells were maintained in anincubator at 37 °C with 5% CO_2. Similarly, normal human umbilical vein endothelial cells (HUVECs) were also cultured at same conditions.

2.5 Exposure of cells to NPs and MTT Bioassay

A stock solution of obtained NPs at 1 mg/mL was prepared using a culture medium (DMEM) as a solvent. This solution was sonicated at 40 kHz for 30 min to avoid NP aggregation. In each sample, the stock solution was diluted to varying concentrations (1.5, 5, 10, 25, 50, 100, 200, and 300 µg/m). A 96-well plate with 1 x 10^5 cells/mL was incubated at 37°C with 5% CO_2 for 24 h. Then, the cells were treated to varying concentrations (1.5–300 µg/mL) at 37°C with 5% CO_2. Then, a 10 µL of MTT solution was added into each well and placed to incubate for 3 h. At last, a volume of 100 µL of Dimethyl sulfoxide (DMSO) was utilized to solubilize the live cell formazan crystals present in each well. The cytotoxicity of NPs was determined by formazan solution absorbance at 570 nm.

2.6 Statistical Analysis

ANOVA-way was successfully used in statistical analysis to establish the significance of the observed differences. P-value ($P < 0.05$) indicates statistical significance.

3. Results and Discussion

3.1 Crystallographic Structure

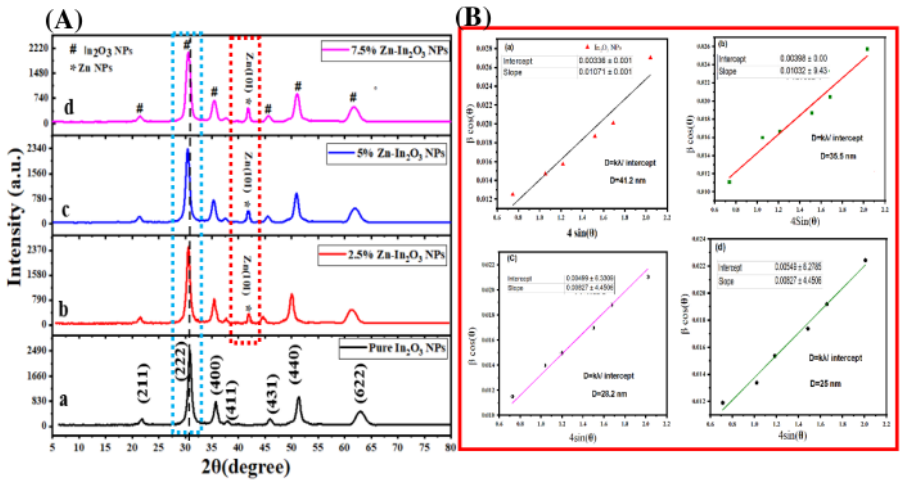

Figure 1. XRD spectra (A): undoped In_2O_3 NPs (A), Zn (2.5%)-In_2O_3 NPs (b), Zn (5%)-In_2O_3 NPs (c), Zn(7.5%)-In_2O_3 NPs (d), and Williamson-Hall (W-H) plot (B): undoped In_2O_3 NPs (A)and Zn (2.5%)-In_2O_3 NPs (b), Zn (5%)-In_2O_3 NPs (c), and Zn(7.5%)-In_2O_3 NPs (d),

Figure 1A(a-d) demonstrates the XRD spectra of undoped In_2O_3 NPs and Zn (2.5%, 5%, 7.5%)-doped In_2O_3 NPs. In undoped In_2O_3 NPs, XRD peaks at 2θ values were located at 21.7°, 30.8°, 35.7°, 37.9°, 45.6°, 51.3°, and 62.8°, corresponding to the cubic bixbyite structure of (211), (222), (400), (411), (431), (440) and (622) planes. Furthermore, It can be seen in (Figure 1b), the new peak (101) plane at 42° is related to Zn metal. The shift of peaks to lower angles (2θ) compared to the undoped In_2O_3 NPs indicates the incorporation of Zn into the In_2O_3 lattice as agreed with earlier studies (Huang and Lin, 2012; Samerjai et al., 2016). This shifted could be attributed to Zn ionic radii (0.074 nm) smaller than In ionic radii (0.122 nm)(Ahmed et al., 2021; Alahsab et al., 2023). Similarly, the XRD spectra of Zn (5% and 7.5%)-doped In_2O_3 NPs (Figures 1A(c and d)) displayed changes in

peak positions and intensities that increased with increasing concertation of Zn doping. These variations were associated with the changes in the crystallographic arrangement outstanding to the existence of Zn in the In_2O_3 lattice (Li et al., 2014; Martha et al., 2014). Furthermore, the In_2O_3 NPs XRD pattern has been matched to the cubic crystal structure (JCPDS card on 01-089-4595)(Koo et al., 2014; Zhang and Zhang, 2012). Using the XRD parameters, the average crystal sizes of the NPs were further estimated by the Scherrer equation. It can be shown in Table 1 that the average crystallite sizes of undoped In_2O_3 NPs and Zn (2.5%, 5%, and 7.5%)-doped In_2O_3 NPs were decreased from 37.2 nm to 18.3 nm with increasing Zn amount as reported with the previous study (Shanmuga Priya et al., 2017). In comparison (Table 1), the average crystallite sizes of undoped In_2O_3 NPs and Zn (2.5%, 5%, 7.5%)-doped In_2O_3 NPs using W-H method were found to be 42.1 nm, 35.5 nm, 28.2 nm, and 25 nm, respectively as displayed in Figure 1B(a-d). XRD results suggested that the Zn doping plays a role in changes in peak positions, intensities, and widths in the In_2O_3 lattice, which influences the crystal structure.

3.2 TEM Analysis

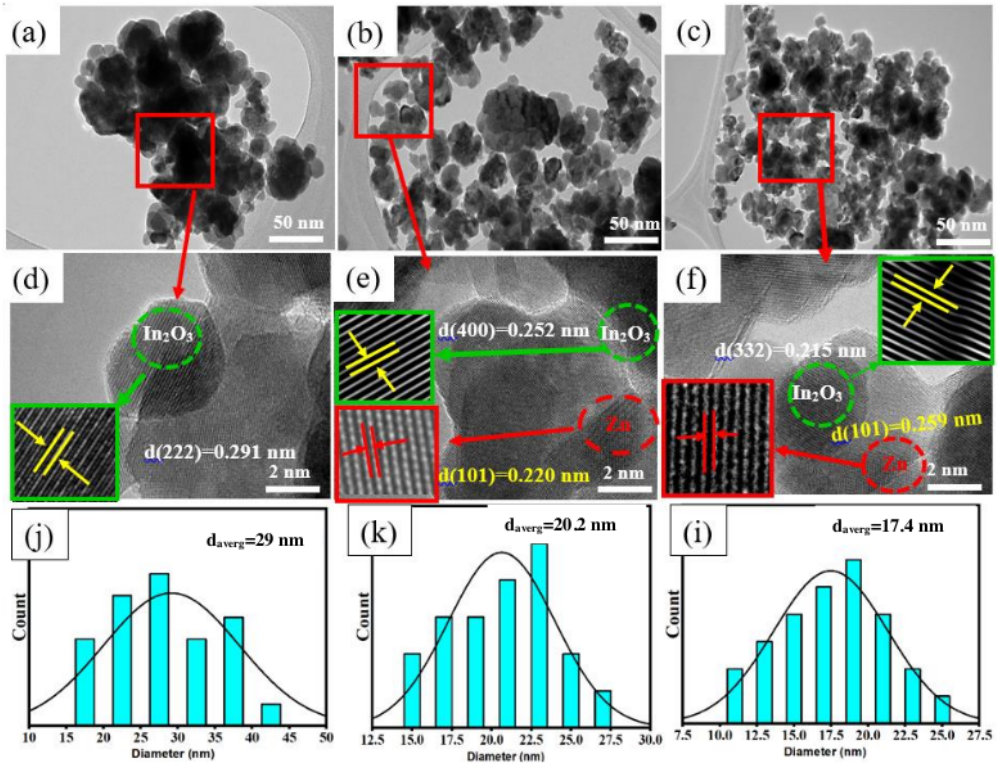

Figure 2. *TEM images of undoped In_2O_3 NPs and Zn(2.5 and 7.5%)- In_2O_3 NPs (a-c), HR-TEM images of undoped and Zn(2.5 and 7.5%)- In_2O_3 NPs (d-f), and the particle size distribution of undoped and Zn(2.5 and 7.5%)- In_2O_3 NPs.*

The growth behavior and morphologies of synthesized samples were further examined using the FETEM technique. As shown in Figure 2(a-c), the particles of Zn (2.5 and 7.5%)-doped In_2O_3 NPs were spherical shape and have less agglomeration and uniform distribution compared to as reported by many investigators (Shokohmanesh and Jamali-Sheini, 2017a). Moreover, HR-TEM images of prepared undoped In_2O_3 NPs and 2.5% and 7.5% Zn-doped In_2O_3 NPs are presented in Figure 2 (d-f), respectively. We observed that d-spacing between adjacent lattice in undoped In_2O_3 NPs and Zn (2.5 and 7.5%)-doped In_2O_3 NPs was 0.291nm, 0.252 nm, and 0.215 nm, matching to the (222), (400), and (332)

plane of In_2O_3, respectively. Additionally, the d-spacing values of the lattice in Zn metal were 0.220 nm and 0.259 nm, corresponding to the (101) planes (Ahamed et al., 2016). These results were in agreement with XRD data (Figure 1A) and our previous study (Z. M. Alaizeri et al., 2022). Figure 2(j-i) depicts in the histogram of particles the size distribution of In_2O_3 NPs and 2.5% and 7.5% Zn-doped In_2O_3 NPs. Table 1 showed that the average particle sizes of synthesized samples decreased (from 29 nm to 17.44 nm) with increasing Zn concentrations, as agreed with this study (Shanmuga Priya et al., 2017).

Table 1: The structural properties of undoped In_2O_3 NPs, Zn (2.5%)-In_2O_3 NPs , Zn (5%)-In_2O_3 NPs, Zn(7.5%)-In_2O_3 NPs.

Sample	ScherrerMethod (nm)	W-H(nm) Method	TEM (nm)
In_2O_3 NPs	37.2	41.2	29
Zn (2.5%)-In_2O_3 NPs	30.1	35.5	20.2
Zn (5%)-In_2O_3 NPs	25.4	28.2	18.3
Zn(7.5%)-In_2O_3 NPs	18.3	25	17.4

3.3 SEM with EDX Analysis

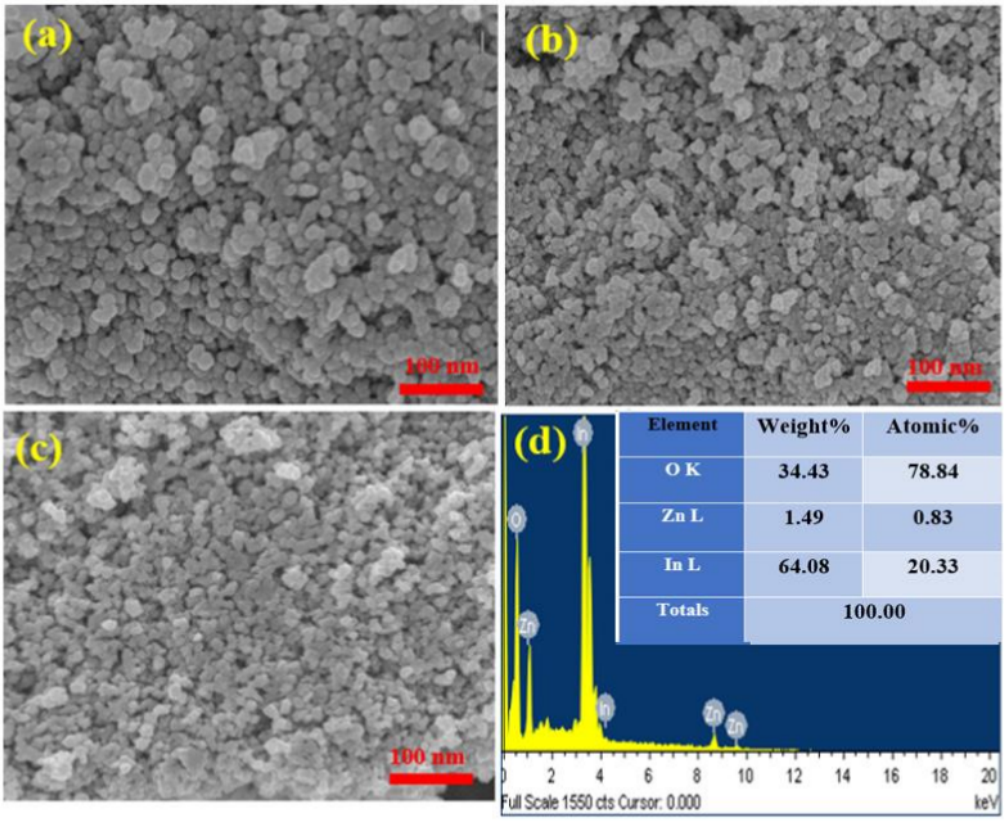

Figure 3. *SEM images of undoped In_2O_3 NPs(a), Zn (2.5%)-doped In_2O_3 NPs (b), Zn (7.5%)-doped In_2O_3 NPs(c), EDX spectra of Zn (7.5 mol%)-doped In_2O_3 NPs (d).*

The SEM images and EDX spectra of undoped In_2O_3 NPs and Zn(2.5% and 7.5%)-doped NPs were presented in Figure 3(a-d). These images provide insights into the shape and morphology of the undoped In_2O_3 NPs and Zn-doped In_2O_3 NPs. Figure 3(a-c) demonstrated that the particles of undoped In_2O_3 NPs were spherical in shape and had high aggregation homogenously compared to 2.5% and 7.5% Zn doped. This suggests that Zn doping at higher concentrations influences the growth and aggregation behavior of undoped In_2O_3 NPs. EDX spectra (Figure 3 d) revealed oxygen (O), zinc (Zn), and indium (In) in Zn(7.5%)-doped In_2O_3 NPs. Besides, the obtained percentages (Figure 3 d) of the elements were good compatibility with the precursor used in the synthesis of 7.5% Zn-doped In_2O_3 NPs. These values agree with XRD spectra (Figure 1A). SEM elemental

mapping (O, Zn, and In) in Zn (7.5%)-doped In_2O_3 NPs is shown in Figure 4(a-d). However, elemental mapping (Figure 4b) confirmed the distribution of oxygen(O), Zinc(Zn), and indium (In) atoms within Zn (7.5%)-doped In_2O_3 NPs. These results indicated that Zn doping in undoped In_2O_3 NPs was successfully prepared. SEM results agreed with XPS results (Figure 5a) and agreed with many studies (Bouhdjer et al., 2016; Inyawilert et al., 2016; Zhu et al., 2020).

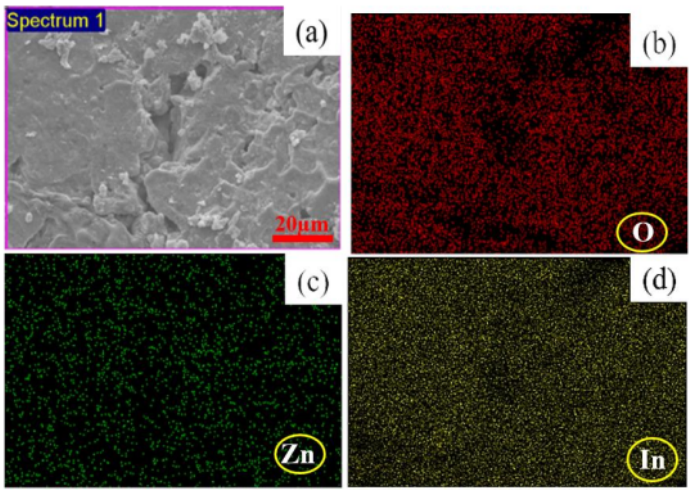

Figure 4. *SEM elemental mapping of Zn(7.5%)- In_2O_3 NPs: Electron image(a), Oxygen(O) (b), Zinc (Zn) (c), Indium (In) (d).*

3.4 XPS Analysis

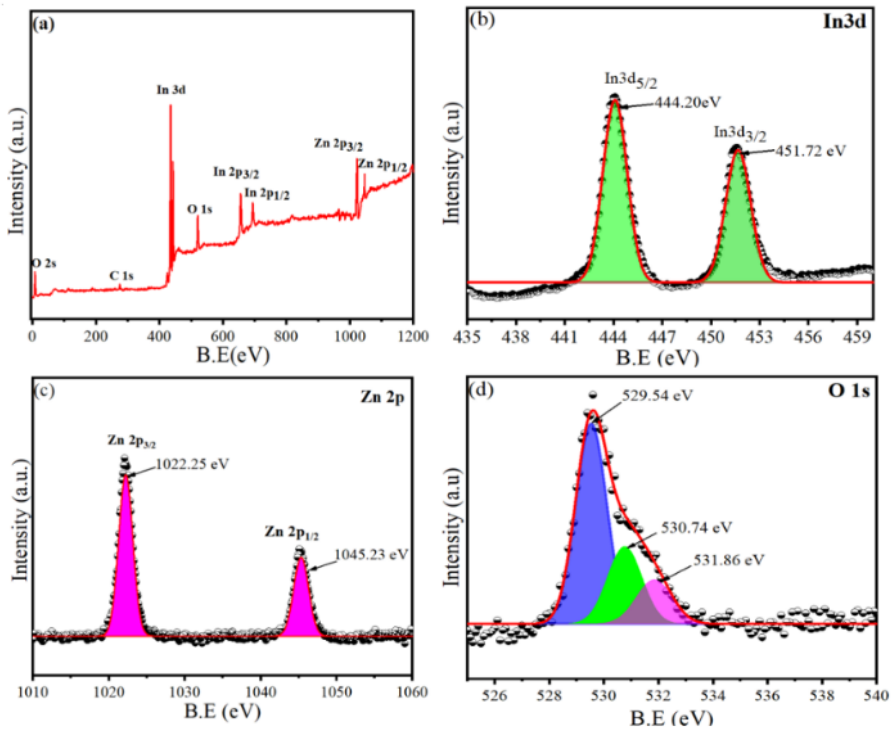

Figure 5. *XPS Characterization of Zn (7.5mol%)-doped In_2O_3 NPs: (a) Full scan of XPS spectra, (b) XPS spectra of In3d, (c) XPS spectra of Zn2p, and (d) XPS spectra of O 1s.*

Figure 5a shows the full scan of XPS spectra that revealed distinct peaks corresponding to In, Zn, and O elements. Furthermore, this spectrum confirmed the successful incorporation of Zn dopants into the In_2O_3 NPs. Figure 5(b-d) showed that the high-resolution spectra were performed to determine the binding energies (B.E) and chemical states of In 3d, Zn 2p, and O 1s elements. As displayed in Figure 5b, the In3d spectra showed typical doublets for $In3d_{5/2}$ and $In3d_{3/2}$ at 444.20 and 451.72 eV, respectively, which provided with prior investigations (Khan et al., 2020; Zhang et al., 2016). The primary peaks found at 1022.25 eV and 1045.23 eV within the Zn 2p spectra (Figure 5b) were associated with the $Zn\ 2p_{3/2}$ and $Zn\ 2p_{1/2}$ peaks, respectively. These peaks distinctly represent Zn^{2+}, which serves as a characteristic feature indicating the oxidation state of Zn in prepared Zn-doped In_2O_3 NPs (Sahai and Goswami, 2015). Figure 5d illustrates XPS spectra of the O1s that exhibited three distinct peaks at 529.54 eV, 530.74 eV, and 531.86 eV. The peak at 529.54 eV is associated with the characteristic lattice

oxygen (O_2^-) features originating from the In_2O_3 lattice (Ma et al., 2016). Similarly, the peaks at 530.74 eV and 531.86 eV are ascribed to the oxygen within regions deficient in the crystalline In–Zn–O system (Montazeri and Jamali-Sheini, 2017). XPs results confirmed that Zn dopants into the In_2O_3 NPs were successfully achieved.

3.5 UV-vis Optical Characterization

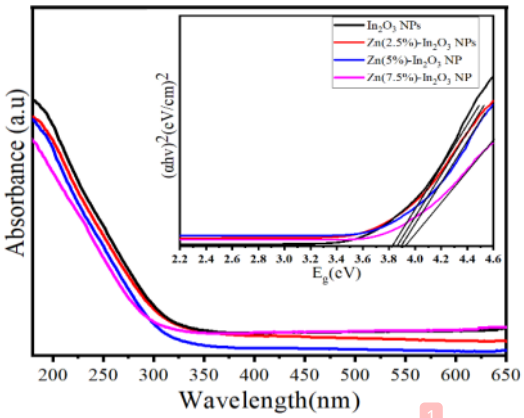

Figure 6. *UV spectra of undoped In_2O_3 NPs and Zn (2.5, 5, and 7.5 mol%)-doped In_2O_3 NPs.*

Figure 6 shows the absorption of UV spectra of both undoped In_2O_3 NPs and Zn (2.5%, 5%, and 7.5%)-doped In_2O_3 NPs. We observed that there is slight shift in the absorption edge of peaks for undoped In_2O_3 NPs and Zn-doped In_2O_3 NPs. This phenomenon of blue shift is a consequence of the wider band gap energy in Zn-doped In_2O_3 NPs. The plot of $(\alpha h\nu)^2$ against photon energy ($E_g=h\nu$) was created (Figure 6) to estimate the band gap energy (Eg) of the NPs. In the present analysis, the energy band gap was estimated using the formula $[(\alpha h\nu)^m=A(h\nu-Eg)]$, where Eg is the band gap energy, A is the transition probability-based constant, and m is optical absorption power index (m = 2). We observed that the band gap energies of undoped In_2O_3 NPs and Zn (2.5%, 5%, and 7.5 mol %)-doped In_2O_3 NPs were 3.83 eV, 3.86 eV, 3.90 eV, and 3.93 eV, respectively. The band gap values indicate a gradual increase in band gap energy with increasing Zn. However, when Zn doped in In_2O_3 NPs, the electronic states to the band structure of In_2O_3 NPs are created. Thus, dopant-induced states are caused by the transition between the valance and conduction bands of highest occupied molecular orbitals (HOMO) and lowest unoccupied (LUMO) orbitals(Amini et al., 2014). Due to this transition between HOMO and LUMO

orbitals Zn-doped In_2O_3 materials can generate and separate electron-hole pairs efficiently, making them excellent for photocatalytic and anticancer applications. Our results were good matched in from prior examinations (Ahamed et al., 2016; Shanmuga Priya et al., 2017; Shokohmanesh and Jamali-Sheini, 2017b).

3.6 PL Analysis

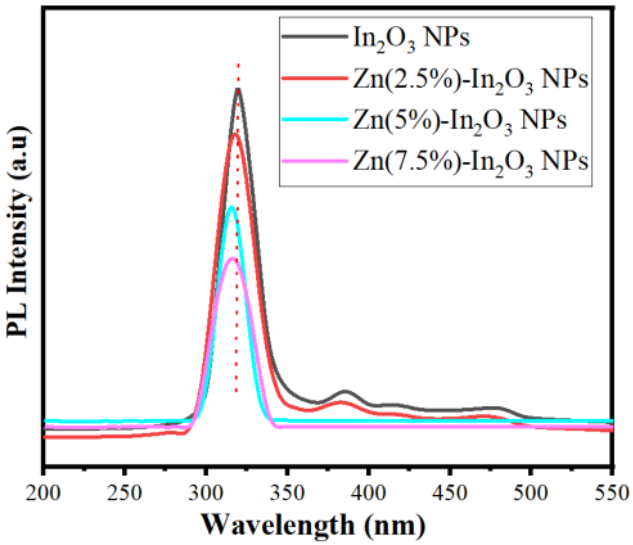

Figure 7. *PL spectra of undoped In_2O_3 NPs and Zn (2.5, 5, and 7.5 mol%)-doped In_2O_3 NPs.*

Figure 7 displays the PL spectra of undoped In_2O_3 NPs and Zn-doped In_2O_3 NPs at 300 nm excitation wavelength. PL spectra showed that emission peaks of undoped In_2O_3 NPs and Zn (2.5, 5, and 7.5 mol%)-doped In_2O_3 NPs were 322.8 nm, 321.3 nm, 318 nm, and 315.2 nm, respectively, corresponding to their band gap energy. This shift in emission peaks is attributed to addition of Zn ions in the In_2O_3 crystal lattice (Singh et al., 2010). Besides, the weak emission peaks were assigned at around 390.1 nm and 415 nm, which could be owing to the existence of oxygen vacancies or interstitial zinc ions (Saikia et al., 2015). A significant shift to a lower wavelength was further observed with the addition of Zn ions. Likewise, there is a significant decrease in the Peak emission intensity with increasing Zn concertation due to occupying Zn^{2+} ions instead of O_2^- ion sites in the In_2O_3 crystal lattice (Alexandrov et al., 2020). PL emission spectra were good, in agreement with

an earlier study (Almontasser and Parveen, 2020). These results indicated that the Zn-doped In_2O_3 NPs can be used in enhanced photocatalytic and anticancer performance.

3.7 Cytotoxicity Study

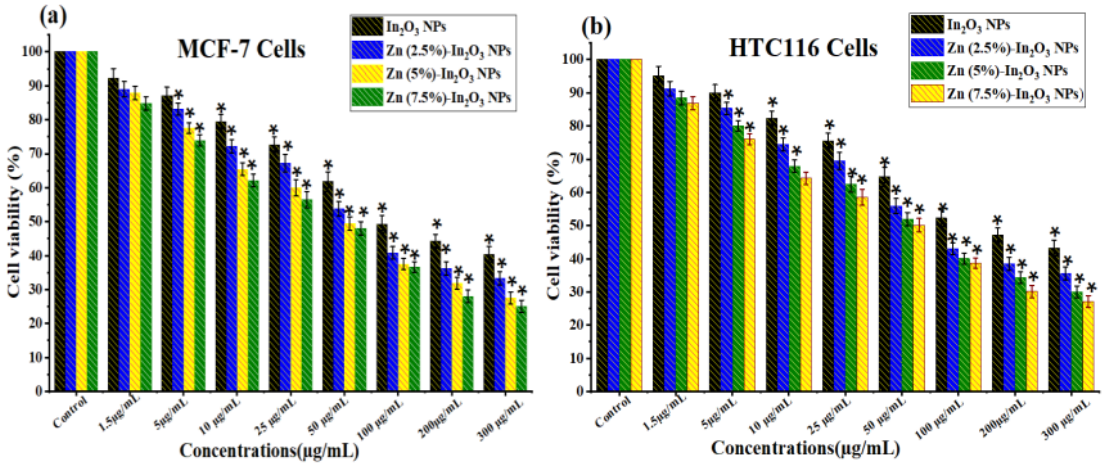

Figure 8. *Cellular viability assessment of undoped In_2O_3 NPs and Zn (2.5%, 5%, and 7.5mol%)-doped In_2O_3 NPs using the MTT Assay: Cell viability in (a) MCF-7 cells and (b) HCT116 cells following exposure to different Concentrations (1.5-300 µg/mL) of each NPs for 24 h. * shows a statistically significant difference from the control group ($p < 0.05$).*

Several oxide NPs with metal ions are attracted to potential uses for cancer therapy applications (Du et al., 2022; Fu et al., 2017; Vinardell and Mitjans, 2018). Figures 8(a and b) illustrate the cell viability of MCF-7 and HCT116 cells using the MTT assay for undoped In_2O_3 NPs and Zn-doped In_2O_3 NPs. As shown in Figure 8a, both undoped In_2O_3 NPs and Zn-doped In_2O_3 NPs exhibited a dose-dependent cytotoxicity influence toward MCF-7 cancer cells. Results exhibited (Figure 8a) that the cytotoxicity effect of undoped In_2O_3 NPs against MCF-7 cancer cells was increased proportionally with increasing amounts of Zn doping. Similarly, the Zn-doped In_2O_3 NPs induced high cytotoxicity (Figure 8b) at higher concentrations toward HCT116 cells than undoped In_2O_3 NPs. Notably, the inhibitory concentration (IC_{50}) for undoped In_2O_3 NPs and Zn-doped In_2O_3 NPs on MCF-

7 and HCT116 cancer cells were shown in Figure 9. It shows that breast cancer cells (MCF-7) exhibited more sensitivity to the cytotoxic effects of both undoped and Zn-doped In_2O_3 NPs compared to HCT116 cells. These results suggest that the anticancer efficacy of Zn-doped In_2O_3 NPs enhanced in comparison to In_2O_3 NPs owing to Zn^{2+} ion addition.

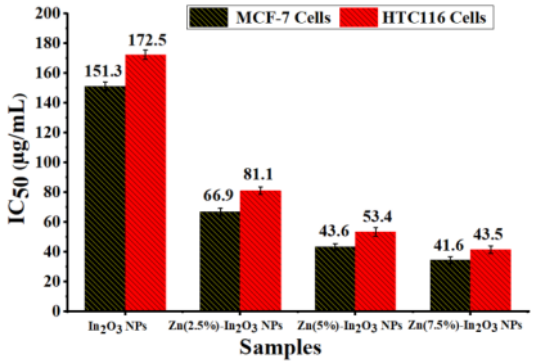

Figure 9. *Inhibitory concentration (IC_{50}) for undoped In_2O_3 NPs and Zn (2.5, 5, and 7.5 mol%)-doped In_2O_3 NPs against two cancer cell lines (MCF-7 and HCT116).*

Our previous studies suggest the potential mechanisms of cancer death by NPs (Ahamed et al., 2021; Z. A. M. Alaizeri et al., 2022) In the present work, Zn-doped In_2O_3 NPs generate reactive oxygen species (ROS) inside cancer cells due react Zn^{2+} ion and In^{3+}ion with molecules of cells (Fenton reaction). Hence, ROS includes a group of chemicals, including superoxide radicals ($O^{\bullet}_2$) and hydrogen peroxide ($^{\bullet}OH$), that exhibit high reactivity. These free radicals can cause oxidative stress and damage DNA, proteins, and lipids. The presence of oxidative stress can potentially induce apoptosis, which is a regulated process of cell death.

3.8 Biocompatibility Study

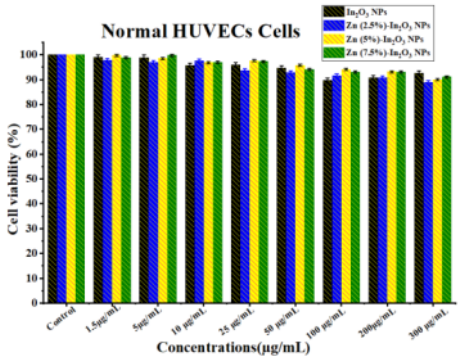

Figure 10. Biocompatibility assay of normal HUVECs for 24 h exposure with different Concentrations (1.5-300 µg/mL) of each undoped In_2O_3 NPs and Zn (2.5%, 5%, and 7.5 mol%)-doped In_2O_3 NPs.

Human normal cells are used to assess the biocompatibility of potential anticancer agents. The present study assessed biocompatibility (Figure 10) on HUVE normal cells at different concentrations (1.5 to 300 µg/mL) for synthesized samples. Figure 10 indicates that the presence of undoped In_2O_3 NPs and Zn (2.5%, 5%, and 7.5%)-doped In_2O_3 NPs did not influence the normal HUVECs. It can be observed that the biocompatibility of In_2O_3 NPs shows enhancement with increasing Zn doping. These results revealed that the Zn (2.5%, 5%, and 7.5%)-doped In_2O_3 NPs can selectively eradicate cancer cells with no effect on normal cells. Based on these results, the biocompatibility of these NPs can be determined by a safe range of concentrations for the potential vivo model. These results were excellent in agreement with previous studies for metal-doped oxide nanoparticles (Ahamed and Khan, 2023; Alaizeri et al., 2021)

4. Conclusions

In this work, the precipitation process was used to effectively produce both undoped In_2O_3 NPs and Zn (2.5, 5, 7.5 mol%)-doped In_2O_3 NPs. The present work showed several advantages of using these NPs for biomedical applications including, including low toxicity, a cost-effective, and scalable approach. This study focused on Zn doping In2O3 NPs to improve their anticancer properties. The physicochemical properties of synthesized materials were investigated using XRD, TEM, SEM, EDX, XPS, UV-Vis, and PL

spectroscopy. XRD analysis showed that Zn doping affected the crystalline structure and phase composition of produced undoped In_2O_3 NPs. TEM and SEM analysis show that The produced NPs exhibited spherical morphology and homogeneous distribution. The elements (Zn, In, and O) and their distribution in Zn-doped In_2O_3 NPs were verified by EDX and XPS analysis. UV-Vis data showed that the band gap energies of prepared samples were increased from 3.38 eV to 3.93 eV with increasing Zn amount. PL peak emissions of prepared samples were observed at around 322.5 nm, 390.1 nm, and 417.6 nm. These emissions were due to the existence of different oxygen vacancies. MTT analysis demonstrated that the cytotoxicity of undoped In_2O_3 NPs against MCF-7 and HCT116 cancer cells was increased with increasing Zn concentration, while normal human cells (HUVECs) did not affect. These results reveal that Zn doping plays a role as therapeutic agent in cancer therapy. The results suggest that these NPs could hold promise as a targeted therapeutic strategy in vivo model.

Consent to participate or publication: N/A**.**

Availability of data and materials: Available when requested.

Declarations: This manuscript is an original investigation; also, it is not submitted elsewhere for publication.

Competing interests: There are no competing interests.

Acknowledgment:

The authors sincerely thank researchers for supporting project number (RSPD2023R813), King Saud University, Riyadh, Saudi Arabia, for funding this research.

References

Ac ce d M us, 2019. 0–10.

Ahamed, M., Akhtar, M.J., Khan, M.A.M., Alaizeri, Z.M., Alhadlaq, H.A., 2021. Facile Synthesis of Zn-Doped Bi2O3 Nanoparticles and Their Selective Cytotoxicity toward Cancer Cells. ACS Omega 6, 17353–17361.

Ahamed, M., Khan, M.A.M., 2023. Enhanced Photocatalytic and Anticancer Activity of Zn-Doped BaTiO3 Nanoparticles Prepared through a Green Approach Using Banana Peel Extract. Catalysts 13, 985. https://doi.org/10.3390/catal13060985

Ahamed, M., Khan, M.A.M., Akhtar, M.J., Alhadlaq, H.A., Alshamsan, A., 2016. Role of Zn doping in oxidative stress mediated cytotoxicity of TiO 2 nanoparticles in human breast cancer MCF-7 cells. Sci. Rep. 6, 1–11. https://doi.org/10.1038/srep30196

Ahmed, A.A.A., Alahsab, E.A.A., Abdulwahab, A.M., 2021. The influence of Zn and Mg doping on the structural and optical properties of NiO nano-structures for optoelectronic applications. Results Phys. 22, 103938. https://doi.org/10.1016/j.rinp.2021.103938

Alahsab, E.A.A., Ahmed, A.A.A., Abdulwahab, A.M., 2023. Synthesis, Structural, Optical and Electrical Properties of Pure and Doped NiO Nanostructures Prepared via The Co-precipitation Method. Thamar Univ. J. Nat. Appl. Sci. 8, 56–69. https://doi.org/10.59167/tujnas.v8i1.1491

Alaizeri, Z.A.M., Alhadlaq, H.A., Aldawood, S., Akhtar, M.J., Ahamed, M., 2022. Photodeposition mediated synthesis of silver-doped indium oxide nanoparticles for improved photocatalytic and anticancer performance. Environ. Sci. Pollut. Res. https://doi.org/10.1007/s11356-022-22594-9

Alaizeri, Z.M., Alhadlaq, H.A., Aldawood, S., Akhtar, M.J., Amer, M.S., Ahamed, M., 2021. Facile synthesis, characterization, photocatalytic activity, and cytotoxicity of ag-doped mgo nanoparticles. Nanomaterials 11. https://doi.org/10.3390/nano11112915

Alaizeri, Z.M., Alhadlaq, H.A., Aldawood, S., Javed, M., Maqusood, A., 2022. Photodeposition mediated synthesis of silver - doped indium oxide nanoparticles for improved photocatalytic and anticancer performance. Environ. Sci. Pollut. Res. https://doi.org/10.1007/s11356-022-22594-9

Alexandrov, A., Zvaigzne, M., Lypenko, D., Nabiev, I., Samokhvalov, P., 2020. Al-, Ga-, Mg-, or Li-doped zinc oxide nanoparticles as electron transport layers for quantum dot light-emitting diodes. Sci. Rep. 10, 1–11. https://doi.org/10.1038/s41598-020-64263-2

Almontasser, A., Parveen, A., 2020. Synthesis and characterization of indium oxide nanoparticles. AIP Conf. Proc. 2220. https://doi.org/10.1063/5.0001683

Amini, M.N., Dixit, H., Saniz, R., Lamoen, D., Partoens, B., 2014. The origin of p-type conductivity in ZnM2O4 (M = Co, Rh, Ir) spinels. Phys. Chem. Chem. Phys. 16 6,

2588–2596.

Ayeshamariam, A., Kashif, M., Bououdina, M., Hashim, U., Jayachandran, M., Ali, M.E., 2014. Morphological, structural, and gas-sensing characterization of tin-doped indium oxide nanoparticles. Ceram. Int. 40, 1321–1328. https://doi.org/10.1016/j.ceramint.2013.07.012

Bierwagen, O., 2015. Indium oxide—a transparent, wide-band gap semiconductor for (opto)electronic applications. Semicond. Sci. Technol. 30.

Bouhdjer, A., Saidi, H., Attaf, A., Aida, M.S., JlassI, M., Bouhaf, I., Benkhetta, Y., Bendjedidi, H., 2016. Structural, morphological, optical, and electrical properties of {In2O3} nanostructured thin films. Optik (Stuttg). 127, 7319–7325. https://doi.org/10.1016/j.ijleo.2016.05.035

Darvish, M., Nasrabadi, N., Fotovat, F., Khosravi, S., Khatami, M., Jamali, S., Mousavi, E., Iravani, S., Rahdar, A., 2022. Biosynthesis of Zn-doped CuFe(2)O(4) nanoparticles and their cytotoxic activity. Sci. Rep. 12, 9442. https://doi.org/10.1038/s41598-022-13692-2

Du, H., Akakuru, O.U., Yao, C., Yang, F., Wu, A., 2022. Transition metal ion-doped ferrites nanoparticles for bioimaging and cancer therapy. Transl. Oncol. 15, 101264. https://doi.org/10.1016/j.tranon.2021.101264

Fu, C., Zhou, H., Tan, L., Huang, Z., Wu, Q., Ren, X., Ren, J., Meng, X., 2017. Microwave-{Activated} {Mn}-{Doped} {Zirconium} {Metal}--{Organic} {Framework} {Nanocubes} for {Highly} {Effective} {Combination} of {Microwave} {Dynamic} and {Thermal} {Therapies} {Against} {Cancer}. ACS Nano 12, 2201–2210. https://doi.org/10.1021/acsnano.7b08868

Gao, P., Pan, W., Li, N., Tang, B., 2019. Boosting {Cancer} {Therapy} with {Organelle}-{Targeted} {Nanomaterials}. ACS Appl. Mater. & Interfaces 11, 26529–26558. https://doi.org/10.1021/acsami.9b01370

Huang, B., Lin, J.-C., 2012. Core–shell structure of zinc oxide/indium oxide nanorod based hydrogen sensors. Sensors and Actuators B-chemical 174, 389–393.

Inyawilert, K., Channei, D., Tamaekong, N., Liewhiran, C., Wisitsoraat, A., Tuantranont, A., Phanichphant, S., 2016. Pt-doped {In2O3} nanoparticles prepared by flame spray pyrolysis for {NO2} sensing. J. Nanoparticle Res. 18. https://doi.org/10.1007/s11051-016-3341-1

Jahan, I., 2022. Nanotechnology for {Drug} {Delivery} and {Cancer} {Therapy}, in: Handbook of {Research} on {Green} {Synthesis} and {Applications} of {Nanomaterials}. IGI Global, pp. 338–362. https://doi.org/10.4018/978-1-7998-8936-6.ch015

Karmaoui, M., Leonardi, S.G., Latino, M., Tobaldi, D.M., Donato, N., Pullar, R.C., Seabra, M.P., Labrincha, J.A., Neri, G., 2016. Pt-decorated In2O3 nanoparticles and their ability as a highly sensitive (<10 ppb) acetone sensor for biomedical applications. Sensors and Actuators B-chemical 230, 697–705.

Khan, M.A.M., Siwach, R., Kumar, S., Ahmed, J., Ahamed, M., 2020. Hydrothermal preparation of Zn-doped In2O3 nanostructure and its microstructural, optical, magnetic, photocatalytic and dielectric behaviour. J. Alloys Compd. 846, 156479. https://doi.org/10.1016/j.jallcom.2020.156479

Koo, B.R., Park, I.K., Ahn, H.J., 2014. Fe-doped In2O3/α-Fe2O3 core/shell nanofibers fabricated by using a co-electrospinning method and its magnetic properties. J. Alloys Compd. 603, 52–56. https://doi.org/10.1016/j.jallcom.2014.03.058

Kulkarni, S.C., Patil, D.S., 2016. Synthesis and characterization of uniform spherical shape nanoparticles of indium oxide. J. Mater. Sci. Mater. Electron. 27, 3731–3735. https://doi.org/10.1007/s10854-015-4215-5

Li, H., Chen, Z., Li, J., Liu, Ru, Zhao, F., Liu, Ran, 2020. Indium oxide nanoparticles induce lung intercellular toxicity between bronchial epithelial cells and macrophages. J. Appl. Toxicol. 40, 1636–1646. https://doi.org/10.1002/jat.4023

Li, P., Fan, H., Cai, Y., Xu, M., Long, C., Li, M., Lei, S., Zou, X., 2014. Phase transformation (cubic to rhombohedral): the effect on the {NO2} sensing performance of {Zn}-doped flower-like {In2O3} structures. RSC Adv. 4, 15161. https://doi.org/10.1039/c3ra47467d

Ma, L., Fan, H., Tian, H., Fang, J., Qian, X., 2016. The n-ZnO/n-In2O3 heterojunction formed by a surface-modification and their potential barrier-control in methanal gas sensing. Sensors Actuators B. Chem. Complete, 508–516. https://doi.org/10.1016/J.SNB.2015.08.085

Malini, V.H., B, I., Gunasekhar, R., Prabu, A.A., 2022. A Review on Electrospun PVDF-Doped Metal Oxide Nanoparticles for Sensor Applications. ECS Trans.

Martha, S., Reddy, K.H., Parida, K.M., 2014. Fabrication of {In2O3} modified {ZnO} for enhancing stability, optical behaviour, electronic properties and photocatalytic activity for hydrogen production under visible light. J. Mater. Chem. A 2, 3621. https://doi.org/10.1039/c3ta14285j

Mishra, P.K., Mishra, H., Ekielski, A., Talegaonkar, S., Vaidya, B., 2017. Zinc oxide nanoparticles: a promising nanomaterial for biomedical applications. Drug Discov. Today 22, 1825–1834. https://doi.org/10.1016/j.drudis.2017.08.006

Montazeri, A., Jamali-Sheini, F., 2017. Enhanced ethanol gas-sensing performance of Pb-doped In2O3 nanostructures prepared by sonochemical method. Sensors Actuators, B Chem. 242, 778–791. https://doi.org/10.1016/j.snb.2016.09.181

Naik, M.Z., Salker, A. V, 2017. A systematic study of cobalt doped In2O3 nanoparticles and their applications. Mater. Res. Innov. 21, 237–243.

Navya, P.N., Kaphle, A., Srinivas, S.P., Bhargava, S.K., Rotello, V.M., Daima, H.K., 2019. Current trends and challenges in cancer management and therapy using designer nanomaterials. Nano Converg. 6. https://doi.org/10.1186/s40580-019-0193-2

Patel, S., Nanda, R., 2015. Nanotechnology in {Healthcare}: Applications and

{Challenges}. Med. Chem. (Los. Angeles). 05. https://doi.org/10.4172/2161-0444.1000312

Sahai, A., Goswami, N., 2015. Structural and optical investigations of oxygen defects in zinc oxide nanoparticles. AIP Conf. Proc. 1665, 1–4. https://doi.org/10.1063/1.4917664

Saikia, L., Bhuyan, D., Saikia, M., Malakar, B., Dutta, D.K., Sengupta, P., 2015. Photocatalytic performance of ZnO nanomaterials for self sensitized degradation of malachite green dye under solar light. Appl. Catal. A Gen. 490, 42–49. https://doi.org/10.1016/j.apcata.2014.10.053

Samerjai, T., Channei, D., Khanta, C., Inyawilert, K., Liewhiran, C., Wisitsoraat, A., Phokharatkul, D., Phanichphant, S., 2016. Flame-spray-made ZnInO alloyed nanoparticles for NO2 gas sensing. J. Alloys Compd. 680, 711–721.

Shanmuga Priya, B., Shanthi, M., Manoharan, C., Dhanapandian, S., 2017. Synthesis, characterization and photocatalytic activity of pure and Zn-doped In2O3 nanostructures. J. Mater. Sci. Mater. Electron. 28, 12784–12794. https://doi.org/10.1007/s10854-017-7106-0

Shanmuganathan, V., Santhosh Kumar, J., Pachaiappan, R., Thangadurai, P., 2021. Transition metal ion-doped In2O3nanocubes: investigation of their photocatalytic degradation activity under sunlight. Nanoscale Adv. 3, 471–485. https://doi.org/10.1039/d0na00694g

Sharma, A., Saini, A.K., Kumar, N., Tejwan, N., Singh, T.A., Thakur, V.K., Das, J., 2022. Methods of preparation of metal-doped and hybrid tungsten oxide nanoparticles for anticancer, antibacterial, and biosensing applications. Surfaces and Interfaces 28, 101641. https://doi.org/https://doi.org/10.1016/j.surfin.2021.101641

Sheena, P.A.L., Sreedevi, A., Viji, C., Thomas, V., 2019. Nickel oxide/cobalt phthalocyanine nanocomposite for potential electronics applications. Eur. Phys. J. B 92, 1–8.

Shokohmanesh, A., Jamali-Sheini, F., 2017a. Synthesis and transient photocurrent behavior of {Zn}-doped {In2O3} nanorods. Sensors Actuators A Phys. 265, 246–252. https://doi.org/10.1016/j.sna.2017.08.010

Shokohmanesh, A., Jamali-Sheini, F., 2017b. Synthesis and transient photocurrent behavior of Zn-doped In2O3 nanorods. Sensors Actuators, A Phys. 265, 246–252. https://doi.org/10.1016/j.sna.2017.08.010

Singh, N., Yan, C., Lee, P.S., 2010. Room temperature CO gas sensing using Zn-doped In2O3 single nanowire field effect transistors. Sensors Actuators B Chem. 150, 19–24. https://doi.org/https://doi.org/10.1016/j.snb.2010.07.051

Sun, T., Zhang, Y.S., Pang, B., Hyun, D.C., Yang, M., Xia, Y., 2014. Engineered {Nanoparticles} for {Drug} {Delivery} in {Cancer} {Therapy}. Angew. Chemie Int. Ed. n/a--n/a. https://doi.org/10.1002/anie.201403036

Sun, X., Liu, X., Deng, X., Xu, X., 2016. Synthesis of Zn-doped In2O3 nano sphere

architectures as a triethylamine gas sensor and photocatalytic properties. RSC Adv. 6, 89847–89854. https://doi.org/10.1039/c6ra16789f

Vázquez-Olmos, A.R., Gómez-Peralta, J.I., Sato-Berrú, R.Y., FERNÁNDEZ-OSORIO, A.L., 2014. Diluted magnetic semiconductors based on Mn-doped In2O3 nanoparticles. J. Alloys Compd. 615.

Vinardell, M.P., Mitjans, M., 2018. Metal/{Metal} {Oxide} {Nanoparticles} for {Cancer} {Therapy}, in: Nanooncology. Springer International Publishing, pp. 341–364. https://doi.org/10.1007/978-3-319-89878-0_10

Yan, S., Li, Z., Li, H., Wu, Z., Wang, J., Shen, W., Fu, Y.Q., 2018. Ultra-sensitive room-temperature H2S sensor using Ag–In2O3 nanorod composites. J. Mater. Sci. 53, 16331–16344. https://doi.org/10.1007/s10853-018-2789-z

Yang, Y.-C., Niu, J.-S., Liu, W.-C., 2022. Study of a Palladium Nanoparticle/Indium Oxide-Based Hydrogen Gas Sensor. IEEE Trans. Electron Devices 69, 318–324.

Zhang, S., Song, P., Yan, H., Wang, Q., 2016. Self-assembled hierarchical Au-loaded In2O3 hollow microspheres with superior ethanol sensing properties. Sensors Actuators, B Chem. 231, 245–255. https://doi.org/10.1016/j.snb.2016.03.020

Zhang, W.H., Zhang, W. De, 2012. Biomolecule-assisted synthesis and gas-sensing properties of porous nanosheet-based corundum In2O3 microflowers. J. Solid State Chem. 186, 29–35. https://doi.org/10.1016/j.jssc.2011.11.031

Zhao, Q.G., Wang, J., Zhang, Y.P., Zhang, J., Tang, A.N., Kong, D.M., 2018. A ZnO-gated porphyrinic metal-organic framework-based drug delivery system for targeted bimodal cancer therapy. J. Mater. Chem. B 6, 7898–7907. https://doi.org/10.1039/c8tb02663g

Zheng, Q., Lee, J.H., Kim, S.J., Lee, H.S., Lee, W., 2021. Excellent isoprene-sensing performance of In2O3 nanoparticles for breath analyzer applications. Sensors Actuators, B Chem. 327, 128892. https://doi.org/10.1016/j.snb.2020.128892

Zhu, W., Xu, T., Liu, W., Wang, W., Feng, M., Cheng, Y., Li, Y., Tian, Y., Li, X., 2020. High-performance ethanol sensor based on {In2O3} nanospheres grown on silicon nanoporous pillar array. Sensors Actuators B Chem. 324, 128734. https://doi.org/10.1016/j.snb.2020.128734

Zn-Modified In2O3 Nanoparticles: Facile Synthesis, Characterization, and Selective Cytotoxicity against Human Cancer Cells

ORIGINALITY REPORT

19%	15%	18%	2%
SIMILARITY INDEX	INTERNET SOURCES	PUBLICATIONS	STUDENT PAPERS

PRIMARY SOURCES

1	www.ncbi.nlm.nih.gov Internet Source	2%
2	www.mdpi.com Internet Source	2%
3	link.springer.com Internet Source	2%
4	www.nature.com Internet Source	1%
5	ZabnAllah M. Alaizeri, Hisham A. Alhadlaq, Saad Aldawood, Mohd Javed Akhtar, Maqusood Ahamed. " Bi O -Doped WO Nanoparticles Decorated on rGO Sheets: Simple Synthesis, Characterization, Photocatalytic Performance, and Selective Cytotoxicity toward Human Cancer Cells ", ACS Omega, 2023 Publication	1%
6	assets.researchsquare.com Internet Source	

		1 %
7	ZabnAllah M. Alaizeri, Hisham A. Alhadlaq, Saad Aldawood, Mohd Javed Akhtar, Maqusood Ahamed. "One-step preparation, characterization, and anticancer potential of ZnFe2O4/RGO nanocomposites", Saudi Pharmaceutical Journal, 2023 Publication	1 %
8	ZabnAllah M. Alaizeri, Hisham A. Alhadlaq, Saad Aldawood, Mohd Javed Akhtar, Aziz A. Aziz, Maqusood Ahamed. "Photocatalytic Degradation of Methylene Blue and Anticancer Response of In2O3/RGO Nanocomposites Prepared by a Microwave-Assisted Hydrothermal Synthesis Process", Molecules, 2023 Publication	1 %
9	repositorio.upn.edu.pe Internet Source	<1 %
10	pubs.rsc.org Internet Source	<1 %
11	journal.waocp.org Internet Source	<1 %
12	www.researchgate.net Internet Source	<1 %

13	Hisham A. Alhadlaq, Mohd Javed Akhtar, Maqusood Ahamed. "Different cytotoxic and apoptotic responses of MCF-7 and HT1080 cells to MnO2 nanoparticles are based on similar mode of action", Toxicology, 2019 Publication	<1 %
14	Weronika Smok, Marta Zaborowska, Tomasz Tański, Adrian Radoń. "Novel In2O3/SnO2 heterojunction 1D nanostructure photocatalyst for MB degradation", Optical Materials, 2023 Publication	<1 %
15	www.tandfonline.com Internet Source	<1 %
16	Mohammed M. Rahman, Abdul Wahid, M.M. Alam, Abdullah M. Asiri. "Efficient 4-Nitrophenol sensor development based on facile Ag@Nd2O3 nanoparticles", Materials Today Communications, 2018 Publication	<1 %
17	dais.sanu.ac.rs Internet Source	<1 %
18	moam.info Internet Source	<1 %
19	Ningning Zhang, Shilei Xie, Wenlong Wang, Dong Xie, Deliang Zhu, Faliang Cheng. " Ultra-Small Fe N/N-CNTs as Efficient Bifunctional	<1 %

Catalysts for Rechargeable Zn-Air Batteries ", Journal of The Electrochemical Society, 2020
Publication

20	chriskresser.com Internet Source	<1 %
21	www.scielo.br Internet Source	<1 %
22	Changhui Zhao, Jinglong Bai, Huimin Gong, Sheng Liu, Fei Wang. "Tailorable Morphology of Core-Shell Nanofibers with Surface Wrinkles for Enhanced Gas-Sensing Properties", ACS Applied Nano Materials, 2018 Publication	<1 %
23	Chaozhi Wang, Jingqin Cui, Xiaoliang Fang, Nanfeng Zheng. "Regulating the Deposition of Insoluble Sulfur Species for Room Temperature Sodium-Sulfur Batteries", Chemical Research in Chinese Universities, 2021 Publication	<1 %
24	Maqusood Ahamed, Mohd Javed Akhtar, M.A. Majeed Khan, Hisham A. Alhadlaq. "Enhanced Anticancer Performance of Eco-Friendly-Prepared Mo-ZnO/RGO Nanocomposites: Role of Oxidative Stress and Apoptosis", ACS Omega, 2022 Publication	<1 %

25	phcogj.com Internet Source	<1%
26	www.leaparizona.com Internet Source	<1%
27	Haiwei Lai, Xiaoyan Huang, Fanxing Zhou, Ting Song, Shiheng Yin, Guojiang Mao, Bei Long, Atif Ali, Guo-Jun Deng. "Construction of dual active sites on the CuAg plasmonic aerogel for simultaneously efficient photocatalytic CO2 reduction and H2 production", Journal of Colloid and Interface Science, 2022 Publication	<1%
28	Maqusood Ahamed, Mohd Javed Akhtar, MA Majeed Khan, Hisham A Alhadlaq. "SnO2-Doped ZnO/Reduced Graphene Oxide Nanocomposites: Synthesis, Characterization, and Improved Anticancer Activity via Oxidative Stress Pathway", International Journal of Nanomedicine, 2021 Publication	<1%
29	Zhimin Yang, Dongzhi Zhang, Haonan Chen. "MOF-derived indium oxide hollow microtubes/MoS2 nanoparticles for NO2 gas sensing", Sensors and Actuators B: Chemical, 2019 Publication	<1%

30 Bardia Mortezagholi, Emad Movahed, Amirhossein Fathi, Milad Soleimani et al. "Plant-mediated synthesis of silver-doped zinc oxide nanoparticles and evaluation of their antimicrobial activity against bacteria cause tooth decay", Microscopy Research and Technique, 2022 <1%
Publication

31 Jinyu Huang, Jianwei Li, Zhonglei Zhang, Junda Li et al. "Bimetal Ag NP and Au NC modified In2O3 for ultra-sensitive detection of ppb-level HCHO", Sensors and Actuators B: Chemical, 2022 <1%
Publication

32 Orawan Wiranwetchayan, Pipat Ruankham, Wonchai Promnopas, Supab Choopun, Pisith Singjai, Arnon Chaipanich, Somchai Thongtem. "Effect of nanoporous In2O3 film fabricated on TiO2-In2O3 photoanode for photovoltaic performance via a sparking method", Journal of Solid State Electrochemistry, 2018 <1%
Publication

33 Xuewei Yin, Zonghong Li, Chunyi Lyu, Yan Wang et al. "Induced Effect of Zinc oxide nanoparticles on human acute myeloid leukemia cell apoptosis by regulating mitochondrial division", IUBMB Life, 2022 <1%

	Publication	
34	journals.plos.org Internet Source	<1 %
35	Jun Yang, Cuikun Lin, Zhenling Wang, Jun Lin. " In(OH) and In O Nanorod Bundles and Spheres: Microemulsion-Mediated Hydrothermal Synthesis and Luminescence Properties ", Inorganic Chemistry, 2006 Publication	<1 %
36	Yinli Duan, Juanqin Xue, Jianan Dai, Yaru Wei, Chao Wu, Shu-Hao Chang, Jing Ma. "Interface engineering of ZnO/In2O3 Z-scheme heterojunction with yolk-shell structure for efficient photocatalytic hydrogen evolution", Applied Surface Science, 2022 Publication	<1 %
37	aip.scitation.org Internet Source	<1 %
38	ouci.dntb.gov.ua Internet Source	<1 %
39	tesisenred.net Internet Source	<1 %
40	thesis.univ-biskra.dz Internet Source	<1 %
41	Ayman A. Zaki, T.A. Abdel-Baset, Mohammed Khalafalla, Hamza A. Qasem, Mostafa	<1 %

Abboudi, Fahd Al-Wadaani, Ali H. Bashal. "Nickel OxideNanoparticles with and without Metallic Doping: Synthesis Structure, Conductivity, Dielectric, and Optical Properties", Materials Science and Engineering: B, 2023
Publication

---

42 Priyanka Panchal, Devina Rattan Paul, Shubham Gautam, Poonam Meena, S.P. Nehra, Sanjeev Maken, Anshu Sharma. "Photocatalytic and antibacterial activities of green synthesized Ag doped MgO nanocomposites towards environmental sustainability", Chemosphere, 2022 <1 %
Publication

---

43 Gouranga Dutta, Sivakumar Manickam, Abimanyu Sugumaran. "Stimuli-Responsive Hybrid Metal Nanocomposite - A Promising Technology for Effective Anticancer Therapy", International Journal of Pharmaceutics, 2022 <1 %
Publication

---

44 Maqusood Ahamed, M. A. Majeed Khan, Mohd Javed Akhtar, Hisham A. Alhadlaq, Aws Alshamsan. "Role of Zn doping in oxidative stress mediated cytotoxicity of TiO2 nanoparticles in human breast cancer MCF-7 cells", Scientific Reports, 2016 <1 %
Publication

---

45 Yujing Su, Yujing Dong, Linping Bao, Chunhui Dai, Xin Liu, Chengyin Liu, Dongwei Ma, Yushuai Jia, Yu Jia, Chao Zeng. "Increasing electron density by surface plasmon resonance for enhanced photocatalytic CO2 reduction", Journal of Environmental Management, 2022 <1%
Publication

Exclude quotes	On	Exclude matches	Off
Exclude bibliography	On		